Unstructured finite volume solver for the computation of the residence time in the Nador lagoon, Morocco

I. Oubarka, A. Yachouti, I. Kissami, I. Elmahi and E. Deleersnijder

Abstract Using the concepts of the Constituent-oriented Age and Residence time Theory (CART, www.climate.be/cart), we compute timescales related to the water renewal in semi-enclosed domains. The modelling system is based on an Eulerian approach and consists of two coupled model components: (i) the shallow-water equations for the hydrodynamical model and (ii) a transport equation for the passive tracer. The full system is incorporated into a high order finite volume solver on unstructured meshes. Advection is approximated by a Non-Homogeneous Riemann Solver (SRNH) which can handle topography variations. Our objective is to study recirculation problems in the Nador lagoon (Morocco) and in particular measure the residence time of water inside the lagoon. An adequate numerical study would determine the necessity and indeed the eventual location of other passes between the lagoon and the Mediterranean permitting to reduce the residence time of a given tracer.

Ismail Oubarka
LMCS-ENSA, Mohammed I University, Oujda-Morocco, e-mail: ismailoubrka@gmail.com
Ahmed Yachouti
LMCS-ENSA, Mohammed I University, Oujda-Morocco, e-mail: yachoutti@gmail.com
Imad Kissami
MSDA, Mohammed VI Polytechnic University, Benguérir-Morocco, e-mail: imad.kissami@um6p.ma
Imad Elmahi
LMCS-ENSA, Mohammed I University, Oujda-Morocco, e-mail: i.elmahi@ump.ac.ma
MSDA, Mohammed VI Polytechnic University, Benguérir-Morocco, e-mail: imad.elmahi@um6p.ma
Eric Deleersnijder
Université catholique de Louvain, IMMC & ELI, Louvain-la-Neuve, Belgium, e-mail: eric.deleersnijder@uclouvain.be

1 Introduction

Coastal lagoons, especially those poorly connected to the neighboring sea, may retain contaminants for a long time, leading to detrimental consequences for the water quality and ecosystems. Therefore, it is crucial to understand and quantify in detail the processes by which the water of such domains is renewed. The first building block usually consists in estimating the time needed for water particles to leave the lagoon and enter the sea, which is usually referred to as the residence time of a water particle [1, 2].

Water is treated as a continuous medium in the majority of environmental studies. In addition, it is also possible to identify water types or masses by tagging relevant water particles. The associated concentrations are governed by advection-diffusion equations. In a water renewal study, it is generally appropriate to distinguish the original water from the replacement water. The former consists of the water particles that are present in the domain at the initial instant, whilst the latter refers to the water originating from the environment of the domain of interest that progressively replaces the original water. The present work focuses on the original water, which will be dealt with using depth-integrated equations.

The modeling system is composed of two coupled model components : (i) the shallow-water equations for the hydrodynamical model and (ii) a transport equation for the passive tracer. These coupled models provide a hyperbolic system of conservation laws with source terms. The full system is incorporated into a finite volume solver on unstructured meshes. A Non Homogeneous Riemann Solver (SRNH) that can handle the topography variations is used to approximate the advection process. The method is decomposed into two stages, which can be interpreted as a predictor-corrector procedure. In the first stage, the scheme uses the projected system of the coupled equations and incorporates the sign matrix of the flux Jacobian, which results in an upwind discretization of the characteristic variables. In the second stage, the solution is updated using the conservative form of the equations and a particular treatment of the bed bottom to achieve a well-balanced discretization of the flux gradients and the bed source terms [3].

As a real application, we focus on the Nador lagoon which is located in the North-East of Morocco (see Fig. 1). The Nador lagoon is an ecosystem of great biological, ecological and economic interest. It covers an area that exceeds $120\,Km^2$ with a maximum depth of $8\,m$, and is fed by the water of The Mediterranean through a pass known as 'Bokhana', the freshwater waterways, the rejections of the untreated human activities (agriculture and urban water industry: metallurgy, textile, ...), and by the water of a waste water treatment plant.

Our objective is to study water circulations in the Nador lagoon and in particular to evaluate the residence time of water inside the lagoon. The impact of the location of the pass on the residence time of the water will be discussed. Increasing the intensity of the exchanges with the Mediterranean is likely to lead to a smaller residence time, though the difference should depend on the subdomain considered. An adequate numerical study would determine the necessity and indeed the eventual location of other passes between the lagoon and the Mediterranean permitting to reduce the residence time of a given tracer. Consequently, this may provide numerical tools to study the physical environment of the lagoon and assess the development strategy reducing pollution risks in the lagoon.

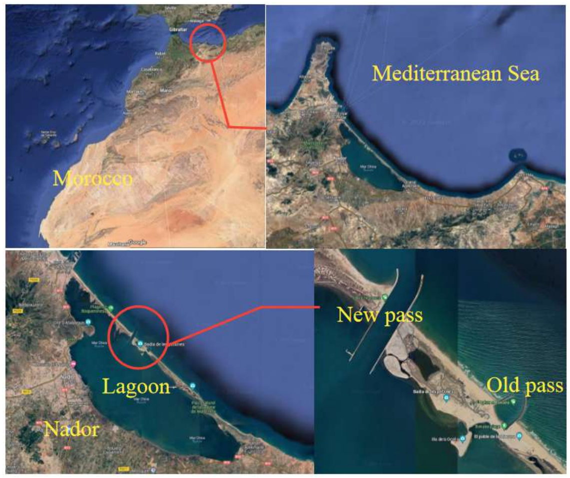

Fig. 1 Location of the Nador lagoon or "Marchica" with zoom on its old and new entrance passes to the lagoon. The old entry pass is currently closed (Image©2021 Google Maps).

2 Mathematical model

2.1 The shallow water equations

Shallow water equations are frequently used to simulate free surface flows that are affected by gravity. These equations which can be derived from the depth-averaged incompressible Navier-Stokes equations, are based on the assumption that the vertical scale is considerably smaller than any typical horizontal scale. For two-dimensional flow problems, the system equations can be written as

$$
\begin{aligned}
&\frac{\partial h}{\partial t} + \frac{\partial (hu)}{\partial x} + \frac{\partial (hv)}{\partial y} = 0 \\
&\frac{\partial}{\partial t}(hu) + \frac{\partial}{\partial x}\left(hu^2 + \frac{gh^2}{2}\right) + \frac{\partial}{\partial y}(huv) = -gh\frac{\partial Z}{\partial x} - \frac{\tau_{bx}}{\rho_w} + \frac{\tau_{wx}}{\rho_w} + \Omega hv + \mathcal{D}_{xx}(h,u,v) \\
&\frac{\partial}{\partial t}(hv) + \frac{\partial}{\partial x}(huv) + \frac{\partial}{\partial y}\left(hv^2 + \frac{gh^2}{2}\right) = -gh\frac{\partial Z}{\partial y} - \frac{\tau_{by}}{\rho_w} + \frac{\tau_{wy}}{\rho_w} - \Omega hu + \mathcal{D}_{yy}(h,u,v)
\end{aligned} \tag{1}
$$

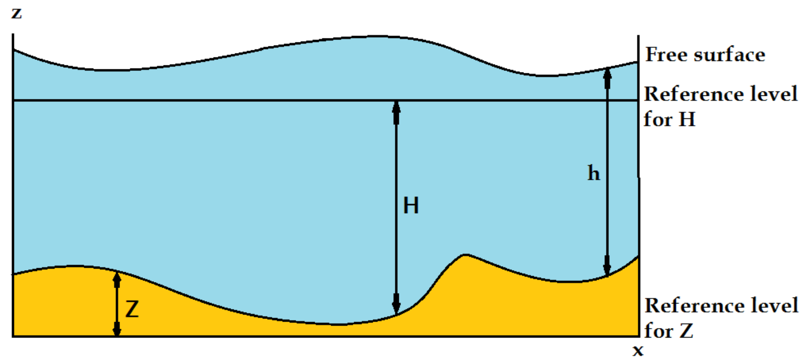

Fig. 2 Presentation of the variables of a shallow flow.

where h is the water depth, g the gravitational acceleration, u and v are the depth-averaged water velocities in x and y direction, Z is the bottom topography. An illustration of these variables is given in Fig.2. Ω is the the Coriolis parameter defined by $\Omega = 2\omega \sin(\phi)$, ρ_w the water density, with ω is the angular velocity of the earth and ϕ is the geographic latitude, τ_{bx} and τ_{by} are the bed shear stress in the x and y direction, respectively, parameterized as follows:

$$\tau_{bx} = \rho_w C_b u \sqrt{u^2 + v^2}, \qquad \tau_{by} = \rho_w C_b v \sqrt{u^2 + v^2} \tag{2}$$

where C_b is the bed friction coefficient, which could be approximated as $C_b = g/C_Z^2$, $C_Z = h^{1/6}/n_b$ is the Chezy constant, with n_b is the bed's Manning roughness coefficient. The surface stress τ_w is often caused by the shear of the wind and is described as a quadratic function of the wind speed.

$$\tau_{w_x} = \rho_a C_w w_x \sqrt{w_x^2 + w_y^2}, \qquad \tau_{w_y} = \rho_a C_w w_y \sqrt{w_x^2 + w_y^2} \tag{3}$$

where ρ_a is the air density and C_w is the coefficient of wind friction and $(w_x, w_y)^T$ is the wind speed at 10 meters above the water's surface. Usually, it is described by

$$C_w = \left(0.75 + 0.067\sqrt{w_x^2 + w_y^2}\right) 10^{-3}$$

For the momentum diffusion terms $\mathcal{D}_{xx}$ and $\mathcal{D}_{yy}$, we used the parameterizations of [4]

$$\mathcal{D}_{xx}(h,u,v) = 2\nu \frac{\partial}{\partial x}\left(h\left(2\frac{\partial u}{\partial x} + \frac{\partial v}{\partial y}\right)\right) + 2\nu \frac{\partial}{\partial y}\left(h\frac{\partial u}{\partial y}\right) \tag{4}$$

$$\mathcal{D}_{yy}(h,u,v) = 2\nu \frac{\partial}{\partial x}\left(h\frac{\partial v}{\partial x}\right) + 2\nu \frac{\partial}{\partial y}\left(h\left(\frac{\partial u}{\partial x} + 2\frac{\partial v}{\partial y}\right)\right) \tag{5}$$

where ν is the kinematic viscosity.

2.2 Residence time formulation

The time that a water parcel takes to exit the region of interest for the first time is known as the residency time $\overline{\theta}$. Therefore, a water parcel's residence time depends on its initial time, initial position, and the region of interest.

Let $\Omega \subset \mathbb{R}^2$ denotes the domain of interest which represents here the lagoon. Its boundary Γ is split into two parts: Γ^c and Γ^p, with $\Gamma = \Gamma^c \cup \Gamma^p$. The first part of the boundary, Γ^c, is impermeable and represents the lagoon-land coastlines. The second Γ^p delineates the open boundary at the "pass" separating the coastal lagoon under study from the neighbouring sea. The outward unit normal vector to the domain boundary is $\mathbf{n}$, with $|\mathbf{n}| = 1$.

To obtain $\overline{\theta}(t_0)$, the mean residence time of the water present in a subdomain Ω' of Ω at time $t = t_0$, one must first obtain the concentration $C(t, \mathbf{x})$ of the passive tracer tagging these water particles. This concentration is the solution of the following partial differential problem [5]

$$\begin{cases} \dfrac{\partial}{\partial t}(hC) + \nabla \cdot (hC\mathbf{u}) = \nabla \cdot (h\mathbf{K}\nabla C) \\ C(t_0, \mathbf{x} \in \Omega') = 1 \\ C(t_0, \mathbf{x} \in \Omega \setminus \Omega') = 0 \end{cases} \tag{6}$$

where $\mathbf{K}$ is the diffusivity tensor of the tracer.

The fact that the original water particles do not cross the coastline boundary leads to the following no-flux boundary condition

$$\left[(hC\mathbf{u} - h\mathbf{K}\nabla C) \cdot \mathbf{n} \right]_{\mathbf{x} \in \Gamma^c} = 0$$

On the interface between the coastal lagoon and the sea, the original water concentration must be prescribed to be zero ($C(t, \mathbf{x} \in \Gamma^p) = 0$) to ensure that the water exits the lagoon and never returns to it again.

Then, the mean residence time in the subdomain Ω' is given by [2]

$$\overline{\theta}(t_0) = \frac{\int_{t_0}^{\infty} \int_{\Omega} h(t, \mathbf{x})\, C(t, \mathbf{x})\, d\mathbf{x}\, dt}{\int_{\Omega} h(t_0, \mathbf{x})\, C(t_0, \mathbf{x})\, d\mathbf{x}} = \frac{\int_{t_0}^{\infty} \int_{\Omega} h(t, \mathbf{x})\, C(t, \mathbf{x})\, d\mathbf{x}\, dt}{\int_{\Omega'} h(t_0, \mathbf{x})\, d\mathbf{x}} \tag{7}$$

One can also define the domain-averaged residence time by setting $\Omega' = \Omega$ in the partial differential problem above. In other words, the domain-averaged residence time is the mean residence time of a passive tracer whose concentration at the initial time $t = t_0$ is equal to unity in the whole domain of interest.

2.3 The global system of PDEs

It is convenient to rewrite (1) and (6) in a compact conservative form.

$$\frac{\partial \mathbf{W}}{\partial t} + \frac{\partial}{\partial x}\left(\mathbf{F}(\mathbf{W}) - \widetilde{\mathbf{F}}(\mathbf{W})\right) + \frac{\partial}{\partial y}\left(\mathbf{G}(\mathbf{W}) - \widetilde{\mathbf{G}}(\mathbf{W})\right) = \mathbf{S}_1(\mathbf{W}) + \mathbf{S}_2(\mathbf{W}) \qquad (8)$$

where $\mathbf{W}$ is the conserved variable's vector, $\mathbf{F}$ and $\mathbf{G}$ are the advective tensor fluxes, $\widetilde{\mathbf{F}}$ and $\widetilde{\mathbf{G}}$ are the diffusion tensor fluxes, $\mathbf{S}_1$ is the source term representing the slope variation. The source term $\mathbf{S}_2$ accounts for coriolis forces, friction losses and wind effects.

$$\mathbf{W} = \begin{pmatrix} h \\ hu \\ hv \\ hC \end{pmatrix}, \quad \mathbf{F}(\mathbf{W}) = \begin{pmatrix} hu \\ hu^2 + \frac{1}{2}gh^2 \\ huv \\ huC \end{pmatrix}, \quad \mathbf{G}(\mathbf{W}) = \begin{pmatrix} hv \\ huv \\ hv^2 + \frac{1}{2}gh^2 \\ hvC \end{pmatrix},$$

$$\mathbf{S}_1(\mathbf{W}) = \begin{pmatrix} 0 \\ -gh\dfrac{\partial Z}{\partial x} \\ -gh\dfrac{\partial Z}{\partial y} \\ 0 \end{pmatrix}, \quad \mathbf{S}_2(\mathbf{W}) = \begin{pmatrix} 0 \\ \Omega hv - \dfrac{\tau_{bx}}{\rho_w} + \dfrac{\tau_{wx}}{\rho_w} \\ -\Omega hu - \dfrac{\tau_{by}}{\rho_w} + \dfrac{\tau_{wy}}{\rho_w} \\ 0 \end{pmatrix}$$

$$\widetilde{\mathbf{F}}(\mathbf{W}) = \begin{pmatrix} 0 \\ 0 \\ 0 \\ hK_x\dfrac{\partial C}{\partial x} \end{pmatrix}, \quad \widetilde{\mathbf{G}}(\mathbf{W}) = \begin{pmatrix} 0 \\ 0 \\ 0 \\ hK_y\dfrac{\partial C}{\partial y} \end{pmatrix},$$

3 Numerical methods

Let's discretize the spatial domain into conforming triangular elements T_i as $\overline{\Omega} = \cup_{i=1}^{N_e} T_i$ and divide the time interval into sub-intervals $[t_n, t_{n+1}]$ with step size Δt. N_e is the total number of elements. We consider the cell-centered finite volume formulation for which each triangle represents a control volume and the state variables are situated at the cell's geometric center. A finite volume discretization of (8) is therefore performed, and can be written, with an explicit Euler scheme for the time, as

$$\mathbf{W}_i^{n+1} = \mathbf{W}_i^n - \frac{\Delta t}{|T_i|} \sum_{j \in N(i)} \int_{\Gamma_{ij}} \mathcal{F}\,(\,\mathbf{W}^n; \mathbf{n})\,\mathrm{d}\sigma + \frac{\Delta t}{|T_i|} \sum_{j \in N(i)} \int_{\Gamma_{ij}} \widetilde{\mathcal{F}}\,(\,\mathbf{W}^n; \mathbf{n})\,\mathrm{d}\sigma$$
$$+ \frac{\Delta t}{|T_i|} \int_{T_i} \mathbf{S}_1(\mathbf{W}^n)\,\mathrm{d}V + \frac{\Delta t}{|T_i|} \int_{T_i} \mathbf{S}_2(\mathbf{W}^n)\,\mathrm{d}V \tag{9}$$

where $\mathbf{W}_i^n$ is the mean value of the solution $\mathbf{W}$ in the control volume T_i at time t_n, $|T_i|$ represents the area of T_i and $N(i)$ is the set of triangles surrounding the cell T_i,

$$\mathcal{F}(\mathbf{W}; \mathbf{n}) = \mathbf{F}(\mathbf{W})n_x + \mathbf{G}(\mathbf{W})n_y \qquad \widetilde{\mathcal{F}}(\mathbf{W}; \mathbf{n}) = \widetilde{\mathbf{F}}(\mathbf{W})n_x + \widetilde{\mathbf{F}}(\mathbf{W})n_y$$

$$\mathbf{W}_i^n = \frac{1}{|T_i|} \int_{T_i} \mathbf{W}^n\,\mathrm{d}V$$

The (SRNH) scheme is formulated by considering only the hyperbolic part of the system (8) and the source term $\mathbf{S}_1$ describing the bed slopes of the domain. The method consists of a predictor stage and a corrector stage, and can be formulated as

$$\mathbf{W}_i^{n+1} = \mathbf{W}_i^n - \frac{\Delta t}{|T_i|} \sum_{j \in N(i)} \mathcal{F}\left(\mathbf{W}_{ij}^n; \mathbf{n}_{ij}\right) |\Gamma_{ij}| + \Delta t \mathbf{S}_{1i}^n$$

$$\mathbf{W}_{ij}^n = \frac{1}{2}\left(\mathbf{W}_i^n + \mathbf{W}_j^n\right) - \frac{1}{2} sgn\left[\nabla\mathcal{F}(\overline{\mathbf{W}}_{ij}^n, \mathbf{n}_{ij})\right]\left(\mathbf{W}_j^n - \mathbf{W}_i^n\right) + \frac{1}{2}|\nabla\mathcal{F}(\overline{\mathbf{W}}_{ij}^n, \mathbf{n}_{ij})^{-1}|\mathbf{S}_{1ij}^n \tag{10}$$

$$\mathbf{S}_{1i}^n = \frac{1}{|T_i|} \int_{T_i} \mathbf{S}_1(\mathbf{W}^n)\,dV$$

where $sgn[\mathbf{A}]$ represents the sign matrix of $\mathbf{A}$ and $\overline{\mathbf{W}}_{ij}^n$ is an averaged state that can be roughly approximated by the mean state or the Roe's average state.

$$\overline{\mathbf{W}}_{ij}^n = \frac{1}{2}\left(\mathbf{W}_i^n + \mathbf{W}_j^n\right)$$

The state $\mathbf{W}_{ij}^n$ is determined by projecting the equations (1) onto the outward normal and tangential coordinates of the local cell, as described in the next section.

3.1 Determination of the sign matrix

We project the shallow water equations onto the local cell's outward normal η and tangential $\tau = \eta^\perp$ to find the sign matrix in equation (10) as follows

$$
\begin{aligned}
\frac{\partial h}{\partial t} + \frac{\partial (hu_\eta)}{\partial \eta} &= 0\\
\frac{\partial (hu_\eta)}{\partial t} + \frac{\partial}{\partial \eta}\left(hu_\eta^2 + \frac{g}{2}h^2\right) &= -gh\frac{\partial Z}{\partial \eta}\\
\frac{\partial (hu_\tau)}{\partial t} + \frac{\partial (hu_\eta u_\tau)}{\partial \eta} &= 0\\
\frac{\partial (hC)}{\partial t} + \frac{\partial (hu_\eta C)}{\partial \eta} &= 0
\end{aligned}
\tag{11}
$$

where the normal and tangential velocities, respectively, are given by the expressions $u_\eta = (u,v).\eta$ and $u_\tau = (u,v).\tau$. In this case, the predictor step in (11) results

$$
\mathbf{U}_{ij}^n = \frac{1}{2}\left(\mathbf{U}_i^n + \mathbf{U}_j^n\right) - \frac{1}{2}sgn\left[\nabla \mathbf{F}_\eta(\overline{\mathbf{U}}_{ij}^n)\right](\mathbf{U}_j^n - \mathbf{U}_i^n) + \frac{1}{2}|\nabla \mathbf{F}_\eta(\overline{\mathbf{U}}_{ij}^n)^{-1}|\mathbf{S}_{1ij}^n \tag{12}
$$

where

$$
\mathbf{U} = \begin{pmatrix} h \\ hu_\eta \\ hu_\tau \\ hC \end{pmatrix}, \qquad \mathbf{F}_\eta(\mathbf{U}) = \begin{pmatrix} hu_\eta \\ hu_\eta^2 + \frac{g}{2}h^2 \\ hu_\eta u_\tau \\ hu_\eta C \end{pmatrix}, \qquad \mathbf{S}_{1ij} = -g\frac{h_i + h_j}{2}\left(Z_j - Z_i\right)\begin{pmatrix} 0 \\ 1 \\ 0 \\ 0 \end{pmatrix}
$$

$\overline{\mathbf{U}}$ is the average state of Roe given by

$$
\overline{\mathbf{U}}_{ij}^n = \frac{h_i + h_j}{2}\begin{pmatrix} 1 \\ \left(\frac{u_i\sqrt{h_i} + u_j\sqrt{h_j}}{\sqrt{h_i} + \sqrt{h_j}}\right)\eta_x + \left(\frac{v_i\sqrt{h_i} + v_j\sqrt{h_j}}{\sqrt{h_i} + \sqrt{h_j}}\right)\eta_y \\ -\left(\frac{u_i\sqrt{h_i} + u_j\sqrt{h_j}}{\sqrt{h_i} + \sqrt{h_j}}\right)\eta_y + \left(\frac{v_i\sqrt{h_i} + v_j\sqrt{h_j}}{\sqrt{h_i} + \sqrt{h_j}}\right)\eta_x \\ \frac{C_i\sqrt{h_i} + C_j\sqrt{h_j}}{\sqrt{h_i} + \sqrt{h_j}} \end{pmatrix}
$$

$sgn\left[\nabla \mathbf{F}_\eta(\overline{\mathbf{U}}_{ij}^n)\right]$ represents the sign of the Jacobian matrix $\nabla \mathbf{F}_\eta(\overline{\mathbf{U}}_{ij}^n)$. It is defined by

$$
\begin{aligned}
sgn\left[\nabla F_\eta(\overline{\mathbf{U}}^n)\right] &= \mathcal{R}(\overline{\mathbf{U}})\, sgn\left[\Lambda(\overline{\mathbf{U}})\right]\, \mathcal{R}(\overline{\mathbf{U}})^{-1}\\
|\nabla F_\eta(\overline{\mathbf{U}}^n)^{-1}| &= \mathcal{R}(\overline{\mathbf{U}})\, |\Lambda(\overline{\mathbf{U}})^{-1}|\, \mathcal{R}(\overline{U})^{-1}
\end{aligned}
\tag{13}
$$

$\mathcal{R}(\overline{\mathbf{U}})$ and $\Lambda(\overline{\mathbf{U}})$ are respectively the eigenvector and eigenvalue matrices of $\nabla\mathbf{F}_\eta(\overline{\mathbf{U}}^n_{ij})$ (see [7] for the details of these matrices).

By incorporating these matrices in the predictor stage (12), the projected state $\mathbf{U}^n_{ij}$ on each edge Γ_{ij} can be easily obtained. The conservative state $\mathbf{W}^n_{ij}$ is then evaluated using the transformations $u = u_\eta n_x - u_\tau n_y$ and $v = u_\eta n_y - u_\tau n_x$

3.2 Treatment of the bed source term

The approximation of the source term in the corrector stage is reconstructed in such a way as to produce the balance between the flux gradients and the bed source term, which is also called the C-property [9, 10]. A numerical method is said to satisfy the C-property if it is compatible with a steady-state solution that is quiescent

$$h_i^n + Z_i^n = h_j^n + Z_j^n = H = constant$$

$$u^n = v^n = 0 \quad \forall T_i, T_j \in \overline{\Omega}, \quad n = 1, 2, 3, \ldots.$$

At the stationary state, the numerical flux in the corrector stage produces

$$\begin{pmatrix} 0 \\ \displaystyle\sum_{j\in N(i)} \frac{1}{2} g (h_{ij}^n)^2 N_{xij} \\ \displaystyle\sum_{j\in N(i)} \frac{1}{2} g (h_{ij}^n)^2 N_{yij} \\ 0 \end{pmatrix} = \begin{pmatrix} 0 \\ \displaystyle -g \int_{T_i} h \frac{\partial Z}{\partial x} dV \\ \displaystyle -g \int_{T_i} h \frac{\partial Z}{\partial y} dV \\ 0 \end{pmatrix} \tag{14}$$

with $N_{xij} = n_{xij}|\Gamma_{ij}|$ et $N_{yij} = n_{yij}|\Gamma_{ij}|$. To approximate the source terms we first split the triangle T_i into three sub-triangles as shown in Fig. 3.

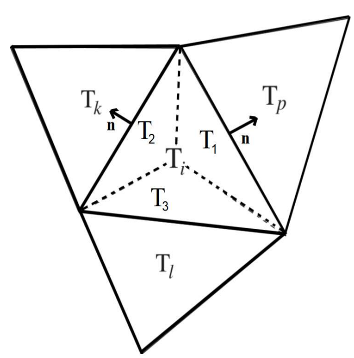

Fig. 3 The decomposition of the control volume T_i.

The source term is then decomposed as

$$\int_{T_i} h\frac{\partial Z}{\partial x}dV = \int_{T_1} h\frac{\partial Z}{\partial x}dV + \int_{T_2} h\frac{\partial Z}{\partial x}dV + \int_{T_3} h\frac{\partial Z}{\partial x}dV \tag{15}$$

where the average values of h on the three sub-triangles T_1, T_2 and T_3 are, respectively, h_1, h_2 and h_3

Using the stationary flow condition on each sub-triangle of T_i and the Gauss divergence formula for the three integrals, the source term reads

$$\int_{T_i} h\frac{\partial Z}{\partial x}dV = -\frac{h_1}{2}h_p N_{x1p} - \frac{h_2}{2}h_k N_{x2k} - \frac{h_3}{2}h_l N_{x3l}$$

for which h_p, h_k and h_l represents the mean values of h on the triangles T_p, T_k and T_l as shown in Fig. 3.

For this reconstruction, the source terms in (14) results in two linear equations for h_1, h_2 and h_3 as follows

$$\sum_{j\in N(i)} (h_{ij}^n)^2 N_{xij} = h_1\left(h_p N_{x1p}\right) + h_2\left(h_k N_{x2k}\right) + h_3\left(h_l N_{x3l}\right) \tag{16}$$

$$\sum_{j\in N(i)} (h_{ij}^n)^2 N_{yij} = h_1\left(h_p N_{y1p}\right) + h_2\left(h_k N_{y2k}\right) + h_3\left(h_l N_{y3l}\right) \tag{17}$$

which are completed by the following conservation equation

$$h_1 + h_2 + h_3 = 3h_i^n \tag{18}$$

After obtaining the average values h_1, h_2 and h_3, the bottom values Z_1, Z_2 and Z_3 are reconstructed in such a way that

$$Z_i + h_i^n = Z_j + h_j^n \quad \text{for} \quad j = 1, 2, 3$$

Finally, the bed slope source term in x-direction is approximated as

$$\begin{aligned}\int_{T_i} h\frac{\partial Z}{\partial x}\,dV = {} & \frac{h_1}{2}\left(Z_p N_{x1p} + Z_2 N_{x12} + Z_3 N_{x13}\right) \\ & + \frac{h_2}{2}\left(Z_k N_{x2k} + Z_1 N_{x21} + Z_3 N_{x23}\right) \\ & + \frac{h_3}{2}\left(Z_l N_{x3l} + Z_1 N_{x31} + Z_2 N_{x32}\right)\end{aligned} \tag{19}$$

And a similar equation is obtained for the approximation of the source term in the y-direction.

With this reconstruction, it is clear that the SRNH scheme is well balanced and preserves the steady state at rest [7].

3.3 Treatment of the friction terms

A fractional semi-implicit approach is used to discretize the friction terms. For example, the momentum equation in the x-direction in the system (1) is divided into two equations as follows

$$\begin{cases} \dfrac{\partial hu}{\partial t} = -n_b^2\, gu \dfrac{\sqrt{u^2+v^2}}{h^{\frac{1}{3}}} \\ \\ \dfrac{\partial hu}{\partial t} + Res(W) = -gh\dfrac{\partial Z}{\partial x} \end{cases} \tag{20}$$

where n_b is the Manning coefficient and $Res(\mathbf{W})$ denotes the convection terms.

First, the upper equation in (20) is integrated using a semi-implicit method, producing

$$\frac{(hu)_i^* - (hu)_i^n}{\Delta t} = -n_b^2\, g(hu)_i^* \frac{\sqrt{(u_i^n)^2 + (v_i^n)^2}}{(h_i^n)^{\frac{4}{3}}} \tag{21}$$

The value $(hu)^*$ is then used as the initial condition in the second step while resolving the second equation in (20) by the (SRNH) method.

3.4 Discretization of diffusion terms

To approximate the diffusion fluxes in the discrete system we used a Green-Gauss diamond reconstruction. This approach was chosen because it is second-order accurate and can be used on general unstructured grids without severe restriction on the regularity of the mesh, and it can be easily incorporated in our finite volume scheme. A co-volume D is first constructed by connecting the barycenters of the elements that share the edge Γ_{ij} and its endpoints as shown in Fig. 4.

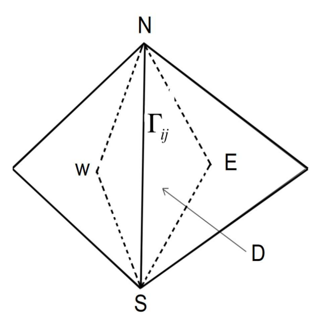

Fig. 4 Diamond shaped co-volume..

Diffusion fluxes in the concentration equation are then evaluated at an inner edge Γ_{ij} as

$$\begin{aligned}\int_{\Gamma_{ij}} hK_x \frac{\partial C}{\partial x} n_x \, d\sigma &= K_x h_{|\Gamma_{ij}} N_{x_{ij}} \frac{\partial C}{\partial x}|_{\Gamma_{ij}} \\ &= K_x h_{|\Gamma_{ij}} N_{x_{ij}} \frac{1}{|D|} \sum_{\varepsilon \in \partial D} \frac{1}{2}(C_{N_1} + C_{N_2}) \int_{\varepsilon} n_x \, d\sigma \quad (22)\end{aligned}$$

where $N_{x_{ij}} = n_{x_{ij}} |\Gamma_{ij}|$. N_1 and N_2 are the nodes of the edge ε of co-volume D, C_{N_1} and C_{N_2} the values of the tracer concentrations at the nodes N_1 and N_2 respectively.

The values C_E and C_W at the barycenters E and W are known and are the cell-centered values, which is not the case for the values at the nodes N and S. To obtain the values at a node N of the mesh, a specific linear interpolation based on the set of cells sharing the vertex N is employed, ensuring weak consistency of the scheme (see [6]).

4 Mesh generation and bed topography

The unstructured meshes in this work are made up of triangles. The mesh of the Nador lagoon created by Gmsh software [8] is displayed in Fig. 5. The computational domain in this study has been restricted to the pass between the lagoon and Mediterranean sea. This will enforce the tidal boundary conditions at this pass. The lagoon's geometry and bed surface topography are irregular and several regions of various depths coexist. In our simulations, the bathymetry was rebuilt using topographical information. This bathymetry is shown in Fig. 6.

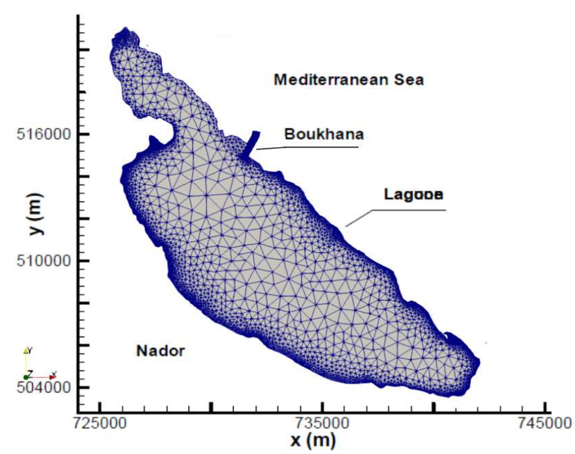

Fig. 5 Unstructured mesh of the Nador lagoon.

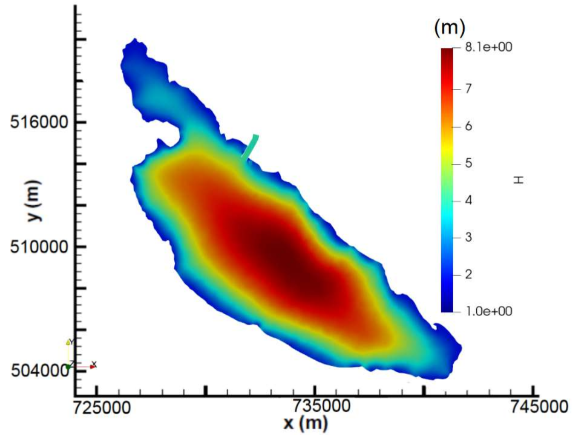

Fig. 6 Bathymetry of the Nador lagoon with its new entrance pass.

5 Numerical setup and results

In this study, the initial assumption is that the flow is stationary with a constant free surface $(h+Z = Cte)$. Additionally, it is important to note that the initial conditions were generated by modeling the shallow water hydrodynamic equations for one year in physical time until the flow was established. After that, the water height and the velocity field are taken as initial state. At this time, the tracer in Nador lagoon is fully released and it's concentration is set to 1. Two types of boundary conditions are specified respectively at the "pass" between the Mediterranean sea and the lagoon noted Γ^p, and at the Nador lagoon coastlines Γ^c. The resulting boundary conditions are:

- At the Nador lagoon coastlines Γ^c:
  - $\overrightarrow{V} = \overrightarrow{0}$ with $\overrightarrow{V} = (u, v)$ is the flow velocity (No-slip conditions) .
  - $\nabla h.n = 0$ (Neumann condition on h)
- At the pass between the Mediterranean sea and the lagoon Γ^p:
  - $\nabla u.n = 0$, $\nabla v.n = 0$ (Neumann conditions on u and v) .
  - $h = H + h_0 + A^* \cos(\omega^* t + \varphi^*)$

H is the depth from a fixed reference level to the bottom, h_0 is a given averaged water elevation taken here equal to $3m$. Initially we have $h = H + h_0$, A^* is the tidal amplitude at the entrance of the lagoon, ω^* is the angular frequency of the tide, and φ^* is the phase of the tide.
In the Nador lagoon, given the fact that the boundary conditions for the water height on Γ^p are time-dependent, they must be updated at each time step as

$$h = H + h_0 + \sum_{i=0}^{N} A_i^* \cos\left(\omega_i^* t + \varphi_i^*\right) \tag{23}$$

For each tidal constituent, the values of the parameters A^*, ω^*, and φ^* are shown in Table. 1.

Table 1 Parameters for the reported tidal waves at the Nador lagoon pass. (reference SLIM code https://www.tpxo.net)

Tidal	Angular frequency ($\circ/s$)	Amplitude (m)	Phase ($\circ$)
M2	8.0511e-03	1.2218e-01	2.8044e+01
S2	8.3334e-03	4.8923e-02	-9.4847e+01
N2	7.8999e-03	2.4840e-02	2.8850e+02
K2	8.3561e-03	1.4412e-02	9.0022e+01
K1	4.1780e-03	4.47471e-02	-1.4758e+02
O1	3.8730e-03	2.3400e-02	-7.2588e+00
P1	4.1552e-03	1.2222e-02	1.9840e+02
Q1	3.7218e-03	2.4141e-03	2.8056e+02
Mm	1.5121e-04	1.0358e-03	1.7292e+02
Mf	3.0500e-04	9.4348e-04	9.1109e+01
M4	1.6102e-02	1.2839e-02	2.8264e+01
Mn4	1.5951e-02	2.5554e-03	-2.1823e+01
Ms4	1.6384e-02	3.3437e-03	2.2460e+02

Over the studied period from January 1 to December 31, 2021, the tidal amplitude fluctuated between $0.21m$ to $0.29m$ (see Fig. 7), which represents a low tidal range (< 0.3 m). This low tidal range is characteristic of the Moroccan Mediterranean Sea both in the open sea and within the lagoon [Hilmi et $al.$, 2003]. The tide is of the semi-diurnal type, represented by the M2 component see Table. 1, as is the case for the Moroccan Atlantic and Mediterranean coasts and the highest tidal amplitudes thus correspond to spring tides Fig. 7.

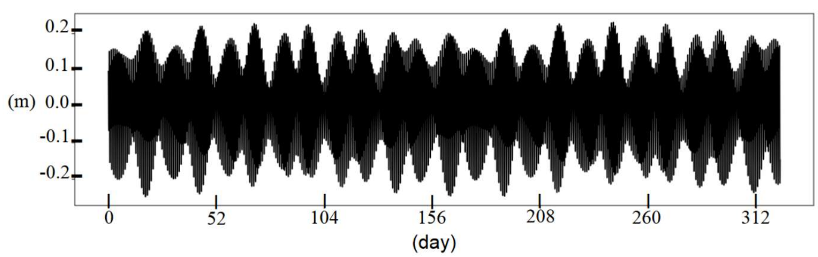

Fig. 7 Tide (in m) set at the entrance of the Nador lagoon pass (35.21°N-2.85°W) from January 1 to December 31, 2021. (Data source: https://www.tpxo.ne).

The wind data taken into consideration in this study are the intensity and the direction in the open sea (35.21°N −2.85°W), established over the period from

January 1 to December 31, 2021 (Data source: https://vortexfdc.com/). The wind intensities vary between $0.1\,m.s^{-1}$ and $18.62\,m.s^{-1}$ with an average intensity of $4.22m.s^{-1}$ and highly variable directions. Fig. 8 summarizes the wind time series from January 1 to December 31, 2021, in the form of a wind rose. It can be seen in this figure that the prevailing winds over the studied period are from sectors blowing in the North-East and South-West sectors (see Fig. 8).

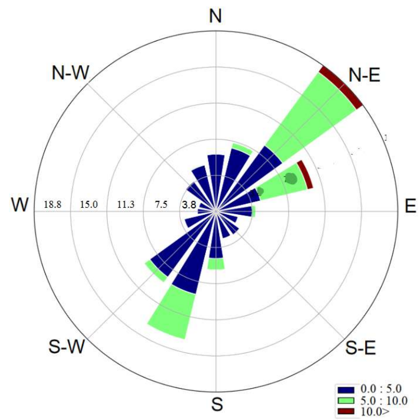

Fig. 8 Wind rose observed over the period from January 1 to December 31, 2021, at the Nador lagoon.

The computations are carried out with a physical time step Δt selected in a way that the following stability condition is met:

$$\Delta t = Cr.\min(\Delta t_{conv}, \Delta t_{diff}) \tag{24}$$

with

$$\Delta t_{conv} = \min_{\Gamma_{ij}}\left(\frac{|T_i| + |T_j|}{2|\Gamma_{ij}|\max_p|\lambda_{ij}^p|}\right), \quad \Delta t_{diff} = \min_{T_i}\left(\frac{|T_i|}{2\max(K_x, K_y)}\right) \tag{25}$$

where λ_{ij}^p is the eigenvalue calculated at the interface Γ_{ij} between the two cells T_i and T_j , and Cr is the current number set to 0.6 to ensure stability of the numerical scheme.

In this study, we will only present the results of the transport of the tracer and the residence time in Nador lagoon by considering various cases of contact with the Mediterranean Sea. Figures 9 and 10 show the results of the simulations of the tracer transport in Nador lagoon considering respectively the new pass, which was used from 2011, and the old pass. Notice that the tracer has been released after one year of hydrodynamical simulations in a physical time in order to obtain situations that are similar to reality of the hydrodynamic in the lagoon. The clear result is that the

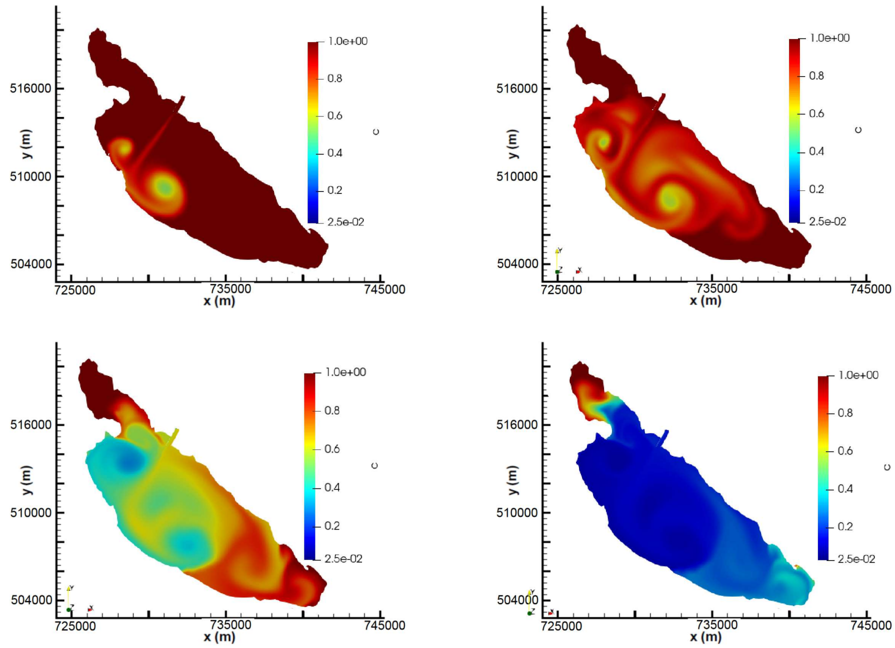

Fig. 9 Tracer concentration in Nador lagoon with the new pass at four different physical times $t = 1, 5, 15, 30$ (day).

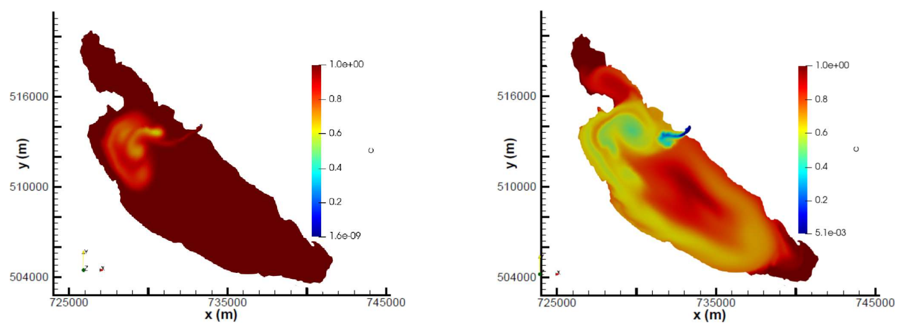

passive tracer leaves the lagoon towards the Mediterranean Sea which is due to the hydrodynamic effect caused by the waves passing through the pass.

Figures 9 and 10 show also that the concentration of the tracer gradually decreases until it completely disappears in the two cases of the connection with the Mediterranean sea. We note that in the case of the new pass, the tracer takes about 48 days to completely disappear from the lagoon, whereas it takes about 6 months in the case of the old pass. This difference is due to the strength and volume of exchanges between the Mediterranean sea and Nador lagoon, which will also greatly affect the residence time in the lagoon.

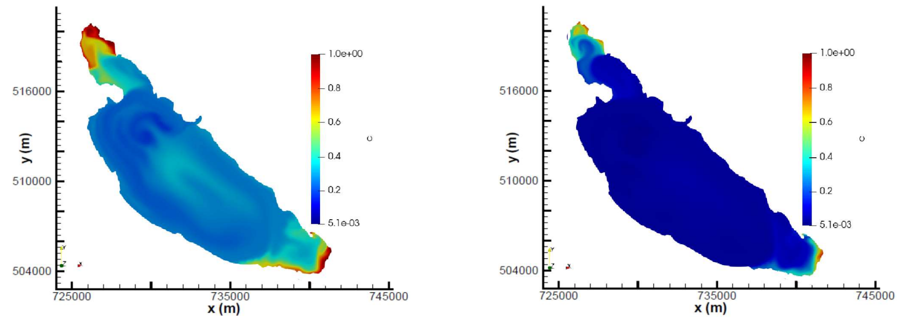

Fig. 10 Tracer concentration in Nador lagoon with the old pass at physical times $t = 2, 30, 90, 180$ (day).

Table 2 The mean residence time of the water present in the Nador lagoon

Type of pass	Initial tide	January-March	April-June	July-September	October-December
New pass	high tides	15.58	14.67	16.82	17.36
	low tides	14.16	13.89	15.02	17.14
Old pass	high tides	58.43	58.10	57.21	61.37
	low tides	57.22	56.73	56.61	59.06

Through the results of the residence time obtained in the Nador lagoon, it is clear that the new pass has increased the strength of the waves entering the lagoon, which caused an increase in the volume of water exchange between the two mediums (Nador lagoon and Mediterranean sea), in contrast to the period when the old pass was relied upon. The hydrodynamics in that period was weak and the water needed a lot of time to renew. The residence time obtained decreased from about 57 days in the case of the old pass, to 15 days in the case of the new pass (see Table. 2). These results are in good agreement with those presented in [11]. In order to understand the influence of the observed winds throughout the year, as well as the effect of the initial time of release of the tracer (high tides and low tides), we have divided the year into 4 periods (January-March, April-June, July-September and October-December). We have then calculated the residence time for each period considering high and low tides cases. The results are presented in Table. 2 and in Fig. 11 where the evolution with time of the relative concentration of the tracer is plotted in the case of the old and the new pass. When the winds blow faster in the direction of the Mediterranean sea, the residence time becomes low, which is not the case when the wind is weak. In addition, the residence time presents some differences in the case of high tides and low tides. In fact, it is always higher when considering low tides (about one day difference between the two cases).

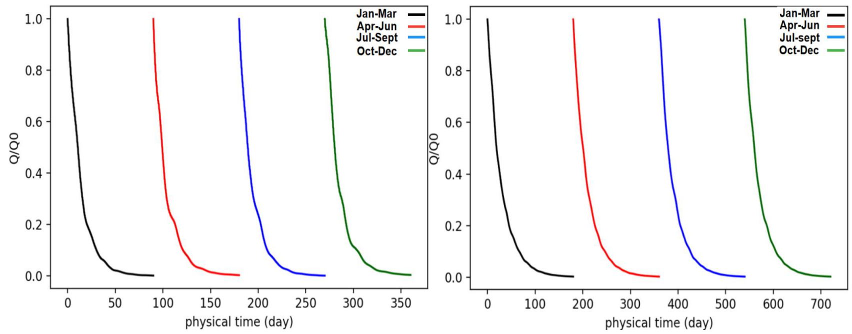

Fig. 11 Temporal distribution of the relative tracer in Nador lagoon with different connection to the Mediterranean sea, new pass (left) and old pass (right).

6 Conclusion

In this work, a robust well balanced finite volume solver has been used to simulate the residence time of the water originally in the Nador lagoon through the new and the old entering pass. The goal is to find a way to renew often the water inside the lagoon and then make it less polluted. Realistic conditions were used for the numerical simulations, which include tidal, wind, bottom friction, and Coriolis forces. The study has demonstrated how the new pass has altered the water circulation within the lagoon, improving the water exchange through the pass and then increasing its renewal. The concentration of the tracer has been highly reduced hroughout the entire lagoon. Furthermore, it has been showed that the exact time at which a tracer is released in a tidal phase affects the residence time in the Nador lagoon. If the tracer is released at high tide, it will stay in the lagoon for a much longer time (approximately 1 day) than if released at low tide. The difference between the time of releasing the tracer could be used to trigger countermeasures to control contaminants from staying in the lagoon for much longer.

References

1. E.J.M. Delhez, Ocean Science **2**, (2006)
2. A. de Brauwere, B. de Brye, S. Blaise, E. Deleersnijder, Journal of Marine Systems **84**, (2011)
3. F. Benkhaldoun, S. Daoudi, I. Elmahi, M. Seaid, Applied Numerical Mathematics **62**, (2012)
4. F. Marche, European J. Mech. B Fluids **26**, (2007)
5. O. Gourgue, E. Deleersnijder, L. White, Estuarine Coastal and Shelf Science **74**, (2007)
6. Y. Coudiere, J.P. Vila, P. Villedieu, in *1st Int. Symp. on Finite Volumes for Complex Applications*, ed. by F. Benkhaldoun & R. Vilsmeier (Hermes, Rouen, 1996), p. 161
7. F. Benkhaldoun, I. Elmahi, M. Seaid, Comput. Methods Appl. Mech. Engrg. **199**, (2010)
8. C. Geuzaine, J.F. Remacle, International Journal for Numerical Methods in Engineering. **79**, (2009)
9. A. Bermúdez, M.E. Vázquez, International Journal of Computers and Fluids **23**, (1994)

10. S. Noelle, N. Pankratz., G. Puppo, J.R. Natvig, J. Comput. Phys. **213**, (2006)
11. F. Maicu, B. Abdellaoui, M. Bajo, A. Chair, K. Hilmi, G. Umgiesser, Continental Shelf Research **228**, (2021)